Towards Contactless, Low-Cost and Accurate 3D Fingerprint Identification

Ajay Kumar, Cyril Kwong

Department of Computing, The Hong Kong Polytechnic University,
Hung Hom, Kowloon, Hong Kong

ajaykr@ieee.org,csmckwong@comp.polyu.edu.hk

Abstract

In order to avail the benefits of higher user convenience, hygiene, and improved accuracy, contactless 3D fingerprint recognition techniques have recently been introduced. One of the key limitations of these emerging 3D fingerprint technologies to replace the conventional 2D fingerprint system is their bulk and high cost, which mainly results from the use of multiple imaging cameras or structured lighting employed in these systems. This paper details the development of a contactless 3D fingerprint identification system that uses only single camera. We develop a new representation of 3D finger surface features using Finger Surface Codes and illustrate its effectiveness in matching 3D fingerprints. Conventional minutiae representation is extended in 3D space to accurately match the recovered 3D minutiae. Multiple 2D fingerprint images (with varying illumination profile) acquired to build 3D fingerprints can themselves be used recover 2D features for further improving 3D fingerprint identification and has been illustrated in this paper. The experimental results are shown on a database of 240 client fingerprints and confirm the advantages of the single camera based 3D fingerprint identification.

1. Introduction

Automated identification of humans is an integral part of infrastructure needed for a wide range of commercial and law-enforcement applications [1], [9]. As compared to other extrinsic biometric features, the fingerprints are considered to be most invariant and employed worldwide by nearly all the law enforcement departments. Traditional fingerprint scans require placing and pressing of fingers against the hard surface, like glass or silicon, and often results in partial or degraded quality images. Such frequent degradation in fingerprint image quality is often attributed to skin deformations, moisture, reside of finger dirt, finger sweat, finger slips, and smear or due to sensor noise [3]. Contactless fingerprint systems can provide hygienic solutions to such problems and can cope-up with the residue of previous fingerprint impressions which can also be a potential security threat.

Contactless fingerprint identification is essentially the acquisition of ridge-valley patterns without any physical contact between the finger and sensor surface [8], [13], [18]. The image quality from such contactless 2D fingerprint sensors [20] is often lower than that of most popular FTIR [1] sensors and its physical size is larger than that of solid-state sensors. Lack of popularity of such contactless 2D fingerprint systems can be attributed to their high cost and bulk as compared to the low-cost legacy touch-based fingerprint devices commonly available today.

1.1. Contactless 3D Fingerprint Identification

In order to avail the benefits of higher user convenience, hygiene, and improved accuracy, contactless 3D fingerprint recognition techniques have recently been introduced [2], [10], [20]-[22]. A contactless fingerprint identification system that uses multiple cameras to systematically acquire multiple views of the presented finger has been detailed in [2], [18]. One of the main obstacles of emerging 3D fingerprint technologies to replace the conventional 2D fingerprint system is their *bulk* and *high cost*, which mainly results from the nature of imaging technologies employed for the 3D fingerprint reconstruction. In [2], [18] five cameras are required while the system in [10] requires a specialized projector and a high-speed camera to implement 3D fingerprint scanning. Therefore there is strong motivation and need to develop low-cost solutions for 3D fingerprint identification.

1.2. Our Work and Contributions

This paper investigates and develops a low-cost solution to the problem of contactless 3D fingerprint identification using *single* camera. Our experimental results presented in this paper illustrate successful use of Lambertian reflectance based *shape from shading* technique for the problem of accurate 3D fingerprint identification. The experimental results are reported on *3D fingerprint database* acquired from the 260 clients. We develop a *Finger Surface Code* representation of 3D fingerprint surface for efficient 3D fingerprint matching (section 3.1). Our experimental results also confirm the superiority of such representation over *Surface Code* representation proposed in [16]. We extend the 2D representation of widely employed 2D minutiae features in 3D space to include height and angle information. Our approach also exploits 2D fingerprint images acquired for 3D fingerprint reconstruction to simultaneously extract 2D minutiae and matches them during identification. Our experimental results illustrate significant improvement in performance using combination of such simultaneously acquired 3D and 2D fingerprint features.
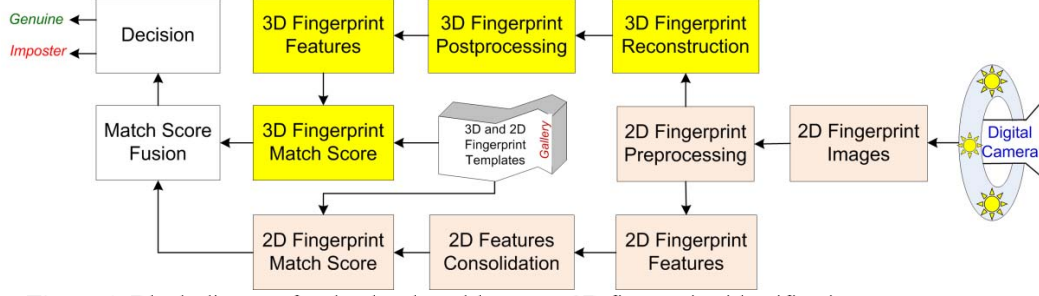
Figure 1: Block diagram for the developed low-cost 3D fingerprint identification system.

2. Block Diagram and Finger Imaging

The finger images are acquired using contactless imaging setup and the average/expected distance between the camera and the finger is ~10 cm. A digital camera which can acquire 2592 × 1944 pixel images with 10 fps (costing less than 100 US$) is employed. We employ 7 symmetrically distributed LED illuminators. Illumination sequence and the image acquisition is synchronized and controlled by a computer using a very low-cost imaging interface (developed by us). The position of LEDs on the acquired images is calibrated. Each of these images are downsampled (after edge detection, boundary scanning, down) to extract 500 × 350 pixels region of interest (ROI).

Once the ROI images are extracted, 3D fingerprint surface is reconstructed using the shape from shading technique. Given 2D image $E'(x, y)$, the shape from shading technique can be used to recover 3D fingerprint surface $z(x, y)$,

$$E(x, y) = \rho I_0 R(p, q) \tag{1}$$

where ρ is the albedo, I_0 is the incident radiance and (p, q) is the surface gradient defined as follows:

$$p = \partial f(x, y)/\partial x, q = (\partial f(x, y))/\partial y \tag{2}$$

The 3D fingerprint surface can be reconstructed by recovering the surface height information $z = f(x, y)$. We approximate and consider finger surface as the Lambertian surface which is illuminated by multiple but calibrated light sources (LED's) $\boldsymbol{l} = [l_x, l_y, l_z]^T$ whose radiance is $\|\boldsymbol{l}\|$. Let $\mathbf{n} = [n_x, n_y, n_z]^T$ be the unit surface normal vectors at some fingerprint surface point of interest. The observed intensity $\mathbf{y}$, from the multiple 2D fingerprint images can be written as follows:

$$\mathbf{y} = \mathbf{L}\,\mathbf{x} \tag{3}$$

where $\mathbf{y} = [y_1, y_2, \dots y_m]^T$, $\mathbf{L} = [l_1, l_2, \dots l_m]^T$, and $\mathbf{x} = \rho[n_x, n_y, n_z]^T$. We assume that the light source directions are not co-planer so that the matrix $\mathbf{L}$ is non-singular. Equation (3) illustrates linear relationship between 3D fingerprint surface, observed pixel intensities from 2D fingerprint image and the unit surface normal vectors $\mathbf{x}$. The unknown vector $\mathbf{x}$ can be estimated from the following equation [15]:

$$\mathbf{x} = (\mathbf{L}^T \mathrm{L})^{-1} \mathbf{L}^T \mathbf{y} \tag{4}$$

The length of recovered vector $\mathbf{x}$ will represent the absolute reflectance (albedo) ρ as $\mathbf{n}$ is a unit vector. The recovered surface normals are then integrated to recover the 3D fingerprint surface $z(x, y)$. The influence of specular reflection from the light source is minimized by eliminating the top 0.228% pixels (outliers) with the high intensity values in seven images acquired for the 3D fingerprint reconstruction.

3. 3D Fingerprint Feature Extraction

The 3D cloud point data reconstructed from the presented fingers is subjected to following (postprocessing) operations for the feature extraction.

(a) Smoothing: The 3D fingerprint surface data is a range data representing the height value (z) on the 2D plane (x, y). The principle curvature calculation is often sensitive to the noise. The smoothing process employed is two steps process; firstly we apply a 5 × 5 median filter on the surface data to suppress the noise. The second step performs Laplacian smoothing [17]. For an vertex P with its neighbors Q_i, the operator

$$U(P) = \frac{1}{\sum_i w_i} \sum_i w_i\, Q_i - P \tag{5}$$

where w_i is the invert distance between Q_i and P as the weight. The new P is defined as; $P_{new} = P_{old} + \lambda U(P_{old})$, where λ is the step size factor. The 3D surface is smoothed after 40 iterations with $\lambda = 0.5$ and the neighbors are chosen in ±2 pixel in x-y directions from P.

(b) Normal Estimation: The normal vector of the data point in the smoothed surface is calculated by the gradient of $z = f(x, y)$. The normal vector is an upward normal with $(-g_x, -g_y, 1)$, where g_x and g_y are the gradient along x and y directions. The normalized surface normal will be used for principle curvature estimation.

(c) Principle Curvature: The principle curvature and the principle direction are computed using Cubic-Order Approximation Algorithm [14]-[15]. For a vertex P, the position of Q_i is transformed to local coordinate that P is (0, 0, 0) and the axes become normal vector of P with two arbitrary orthonormal vectors in the tangent plane. Let (x_i, y_i, z_i) be the position of the vertex and (a_i, b_i, c_i) be the normal vector of the vertex in the transformed coordinate. The Cubic-Order fitting approach tries to locate a surface that can fit the vertex and its neighbors such that,

$$z = f(x, y)$$
$$= \frac{A}{2}x^2 + Bxy + \frac{C}{2}y^2 + Dx^3 + Ex^2y + Fxy^2 + Gy^3$$

The normal vector of the vertex in the approximated surface is written as:

$$N(x, y) = (f_x(x, y), f_y(x, y), -1) \qquad (6)$$
$$= (Ax + By + 3Dx^2 + Exy + Fy^2, \ Bx + Cy + Ex^2 + 2Fxy + 3Gy^2, \ -1)$$

Let $\mathbf{k}$ be the coefficient vector; $\mathbf{k} = (A \ B \ C \ D \ E \ F \ G)^T$. We have three equations for each vertex in the data set:

$$\left(\frac{1}{2}x_i^2 \ x_iy_i \ \frac{1}{2}y_i^2 \ x_i^3 \ x_i^2y_i \ x_iy_i^2 \ y_i^3\right)\mathbf{k} = z_i \qquad (7)$$

$$(x_i \ y_i \ 0 \ 3x_i^2 \ 2x_iy_i \ y_i^2 \ 0)\mathbf{k} = -\frac{a_i}{c_i} \qquad (8)$$

$$(0 \ x_i \ y_i \ 0 \ x_i^2 \ 2x_iy_i \ 3y_i^2)\mathbf{k} = -\frac{b_i}{c_i} \qquad (9)$$

By solving $\mathbf{k}$ with least-square fit on $U\mathbf{k} = \mathbf{d}$, where U is the 3n*7 matrix by the left hand side of the equations above and $\mathbf{d}$ is the vector on the right hand side of the equations above, we can construct following Weigarten curvature matrix of the surface:

$$W = \begin{pmatrix} A & B \\ B & C \end{pmatrix} \qquad (10)$$

The eiganvalues of Weigarten matrix are the maximum and minimum principle curvature of the surface (k_{max}, k_{min}), and their eigenvectors are the principal directions (t_{max}, t_{min}).

3.1. Finger Surface Code Representation

The shape index (*SI*) can be used to describe 3D surface using curvature information and computed as follows [12]:

$$SI = \frac{1}{2} - \left(\frac{1}{\pi}\right)\tan^{-1}\left(\frac{k_{max} + k_{min}}{k_{max} - k_{min}}\right) \qquad (11)$$

When *SI* is close to 0.75, the shape of the surface is more likely to be the ridge shape. On 3D fingerprint surface, the *SI*'s are concentrated in numeric values representing fingerprint valley (0.25) and ridge (0.75) regions. The surface index is therefore likely to be largely distributed in this zone. Therefore our encoding scheme splits the fingerprint surface into five zones: cup, rut, saddle, ridge, cap. The direction of the dominant principle curvature ($\max(|k_{max}|, |k_{min}|)$) is portioned into six directions. Rut and ridge zones are further divided since cup, saddle and cap's $|k_{max}|$ and $|k_{min}|$ are close; therefore, t_{max} and t_{min} are not as accurate as those in rut and ridge zones. The resulting feature representation has 15 different values and therefore 4-bits can store resulting *binary code* for each pixel. This binarized representation of 3D fingerprint surface is referred to as *Finger Surface Code* in this paper and is similar to *FingerCode* [11] or *IrisCode* in [25]. The matching score between two $U \times V$ *Finger Surface Codes* is computed using their normalized Hamming distance as follows:

$$D_{3DCurvature} = \frac{1}{4 \times U \times V}\sum_{p=1}^{U}\sum_{q=1}^{V}\otimes(J(p,q), K(p,q)) \qquad (12)$$

Table 1: The zones of the proposed *Finger Surface Code*.

SI	0 – 0.0625	0.0625 - 0.4375						0.4375- 0.5625	0.5625 - 0.9375						0.9375 - 1
Angle(pi/6)	/	0	1	2	3	4	5	/	0	1	2	3	4	5	/
Code	0	1	2	3	4	5	6	7	8	9	10	11	12	13	14

where $\otimes$ denotes the Hamming distance between the two four bit *Finger Surface Codes*. The 3D fingerprint *surface curvature* matching using *Finger Surface Code* representation has shown to be quite effective (results in figure 2) and also more accurate than *SurfaceCode* representation developed for 3D palmprints in [16].
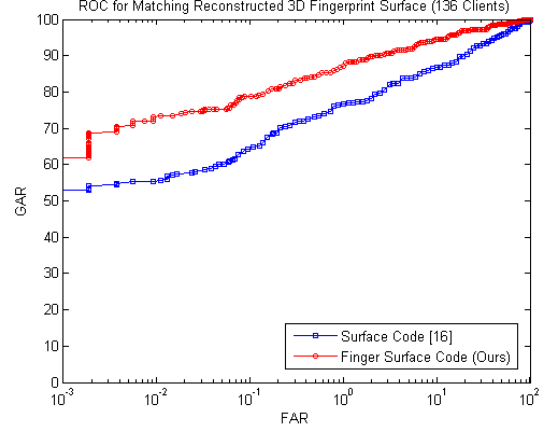

Figure 2: Comparative results to match 3D fingerprint surface curvature from 135 clients reconstructed 3D fingerprints.

3.2. 3D Minutiae Representation and Matching

The 2D fingerprint templates (x, y, θ) typically include position of the minutiae (x, y) and the angle θ representing the orientation of the minutiae in 2D space. This representation can be extended to include *new (extended)* features which can more accurately localize such minutiae in 3D space. The 3D feature z can represent the height of the vertex on the reconstructed 3D fingerprint surface at position (x, y) while the ϕ can represent the minutiae orientation in spherical coordinates with unit length 1. Such extended minutiae templates can more effectively localize the minutiae in 3D space and referred in this paper as 3D minutiae (x, y, z, θ, ϕ). The 3D minutiae matching algorithms developed to robustly match 3D minutiae, say P and Q, from two 3D fingerprints are described in the following. Firstly a reference minutia, each from the template P and template Q, is selected and all the other
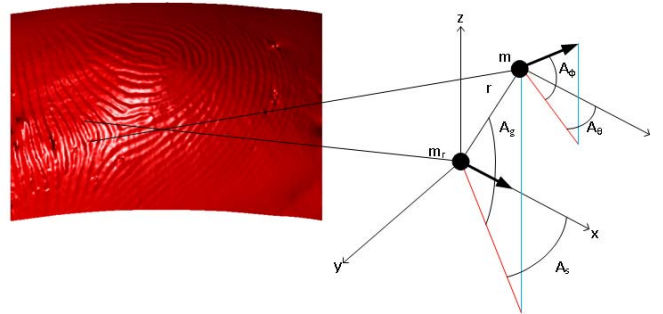

Figure 3: Computing relative localization of two 3D minutiae features in 3D space from the (real) reconstructed 3D fingerprint.

minutiae are transformed to the spherical coordinates. Then the (two) reference minutiae are aligned with the *x*-axes and *z*-axes. This alignment can ensure that the aligned reference minutiae (in both template *P* and *Q*) location can serve as the universal origin/reference (figure 3-4) to measure other minutiae distances in the respective templates. If an aligned minutia is represented as $m_r = [x_r, y_r, z_r, \theta_r, \phi_r]$ in template *P*, the relative representation of other 3D minutiae in template $P^\dagger$, say *m* (see figure 3-4 to visualize *relative* representation of two 3D minutiae), can be denoted as $m = [r, A_s, A_\theta, A_g, A_\phi]$; where *r* is the radial distance with reference minutiae, A_θ, is the azimuth angle and A_ϕ is the elevation angles respectively that localizes minutiae *m* in 3D plane, while A_s and A_g are the azimuth and the elevation angle that localizes the radial vector *r* (with respect to reference minutiae m_r) in 3D space. Let $R_z(\theta)$ and $R_y(\phi)$ be the rotation matrix along *z* and *y* direction in Cartesian coordinate, and sph(*x*, *y*, *z*) be the Cartesian to Spherical coordinate transformation with unit length one. The parameters for the relative representation (feature vector) of minutiae *m* are computed as follows:

$$[x'y'z']^T = R_y(-\phi_r)R_z(-\theta_r)\frac{1}{r}[x - x_r \ y - y_r \ z - z_r]^T$$
$$r = \sqrt{(x-x_r)^2 + (y-y_r)^2 + (z-z_r)^2}, [A_s \ A_g] = \text{sph}([x'y'z']),$$
$$[A_\theta \ A_\phi] = \text{sph}\left(\left(R_y(-\phi_r)R_z(-\theta_r)(\text{sph}^{-1}([\theta \ \phi]))^T\right)^T\right) \quad (13)$$

Two 3D minutiae in the two fingerprint template *P* and *Q* can be considered be matched if the difference between their feature vectors $(r_{Pi}, A_{s_{Pi}}, A_{\theta_{Pi}}, A_{g_{Pi}}, A_{\phi_{Pi}})$ and $(r_{Qi}, A_{s_{Qi}}, A_{\theta_{Qi}}, A_{g_{Qi}}, A_{\phi_{Qi}})$ is smaller than a given threshold or tolerance limit;

$$\Delta r = |r_{Pi} - r_{Qj}|, \ \Delta_{A_s} = \min\left(\left|A_{s_{Pi}} - A_{s_{Qj}}\right|, 360° - \left|A_{s_{Pi}} - A_{s_{Qj}}\right|\right)$$
$$\Delta_{A_\theta} = \min\left(\left|A_{\theta_{Pi}} - A_{\theta_{Qj}}\right|, 360° - \left|A_{\theta_{Pi}} - A_{\theta_{Qj}}\right|\right) \quad (14)$$
$$\Delta_{A_g} = |A_{g_{Pi}} - A_{g_{Qj}}|, \ \Delta_{A_\phi} = |A_{\phi_{Pi}} - A_{\phi_{Qj}}|$$

If $\Delta r \leq th_r$, $\Delta_{A_s} \leq th_{A_s}$, $\Delta_{A_\theta} \leq th_{A_\theta}$, $\Delta_{A_g} \leq th_{A_g}$, and $\Delta_{A_\phi} \leq th_{A_\phi}$, the minutiae pair from templates *P* and *Q* can
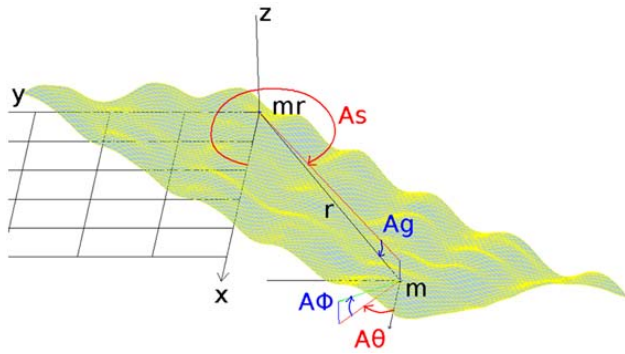

Figure 4: A reference minutiae from one 3D fingerprint template is transformed to origin and used compute relative distance with other minutiae in same/different 3D templates.

---

† Also in template *Q* since the reference minutiae have been aligned to serve as the universal reference/origin.

be considered as matched. The matching score between two 3D minutiae template *P* and *Q* is computed as follows:

$$S_{3DMinutiae} = \frac{m^2}{M_P M_Q} \quad (15)$$

where *m* refers to the total number of 3D matched minutiae pairs and M_P, M_Q is the number of 3D minutiae in template *P* and *Q* respectively.

3.3. Matching 2D fingerprints

The 2D fingerprint images acquired to reconstruct 3D fingerprints, using shape from shading approach, can also be simultaneously matched and used for the performance improvement. Since these 2D images are acquired at-a-distance, the contrast of the intensity between valley and ridge is low. These images require contrast improvement before subjecting them to Gabor filter based fingerprint enhancement algorithm [1]. We employed Homomorphic filtering [2] for such contrast improvement.

Among variety of 2D minutiae extraction algorithms in the literature, the NBIS's MINDTCT function from NIST is available public domain [6] and employed in our work. The fingerprint template generated from the MINDTCT identifies the minutiae as $[x, y, \theta, q]$, where *q* is the quality of the minutia. We used NIST's bozorth3 [6] to generate matching score between the minutiae templates. The maximum score of all reference minutia pair is chosen from the final score of two templates (similar to as also used for generating scores using 3D minutiae in equation 15). Since seven images of the same finger, under different illuminations, are simultaneously acquired and these can be used for generating 2D fingerprint matching score for every client. We use the maximum of the matching scores generated from all such seven images of clients' 2D fingerprints images (corresponding to each 3D fingerprint) to generate final 2D matching fingerprint matching score. As shown from the results in figure 7, such strategy can exploit best of the available information to achieve superior performance.
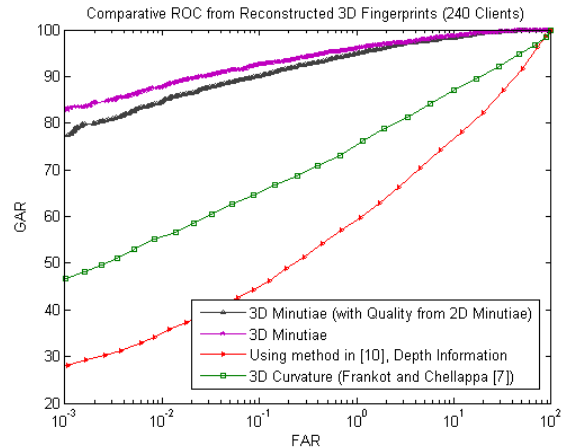

Figure 5: Comparative ROC using 3D fingerprint features from the reconstructed 3D fingerprints.

4. Experimental Results

The proposed approach for the 3D fingerprint identification was evaluated on 3D fingerprint database of 1440 3D fingerprints, reconstructed using 10080 2D fingerprint images, from 240 clients (we refer the 'client' as the distinct finger even if it belongs to same person). In addition, we also acquired (3D fingerprint) images from 20 clients which were employed to compute parameters during the training stage. We acquired six 3D fingerprints from each of the client. This database was acquired from February 2012 to June 2012 and the entire database from 260 clients fingerprint images is being made available [5] for further research. In the best of our knowledge, so far there is no 3D fingerprint database available in the public domain. Therefore the 3D fingerprint matching strategy developed in section 3.1 and 3.2, which is rather generalized for cloud point data from 3D fingerprints, is only evaluated on the acquired 3D fingerprint database.

We explored performance from the 3D fingerprint images reconstructed using several least square solutions. Figure 5 illustrates a typical 3D fingerprint image reconstructed using Frankot and Chellappa algorithm [7]. It was observed that this method of reconstructing 3D fingerprints is most effective in generating accurate results when resulting 3D fingerprints are matched using surface curvature features (figure 5). Our experimental results generated 3600 (240×15) genuine and 2064960 ($240 \times 6 \times 239 \times 6$) impostor matching scores from the six 3D fingerprint images reconstructed from each of the 240 clients. The Poisson solver [19] generates direct analytical results to the least square problem by solving a Poisson equation and has been shown to generate 3D fingerprint surface which has close resemblances to its natural shape. Our experiments for matching recovered 3D minutiae from the 3D fingerprints reconstructed using Poisson solver achieved superior performance than those from the 3D fingerprints reconstructed using [7]. Figure 6 illustrates such comparative results for matching the recovered 3D
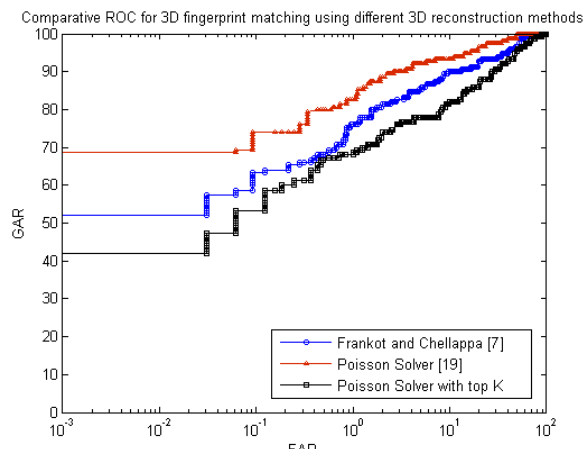

Figure 6: Comparative matching accuracy from the 3D fingerprints reconstructed using different least square solutions.
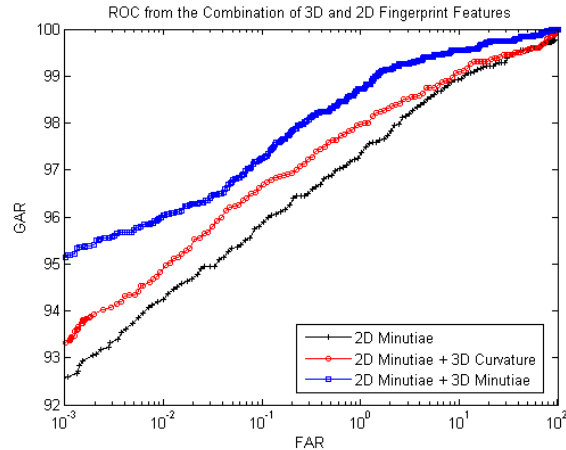

Figure 7: The ROC using combination of 3D fingerprint features with simultaneously recovered 2D fingerprint features.

minutiae from first 10 clients' 3D fingerprints. Therefore this solution was preferred for matching 3D fingerprints using 3D minutiae in further/all experiments.

We also implemented 3D fingerprint matching approach described in [10] using the depth information. The receiver operating characteristics (ROC) using this approach is also shown in figure 5 for comparison. As can be observed from this ROC, the resulting performance (EER of 18.56%) is quite poor. Our database of 3D fingerprints (or 3D model of reconstructing the 3D information) illustrates *larger distortion* after flatting the images than those (flattening in reference [10]) from the structured lighting approach in [10]. Significant degradation in performance (figure 5) from the depth information matching can be attributed to such distortion in the flatting of the 3D fingerprint model. Our 3D fingerprint model does not reconstruct fingerprints as cylinder-like (because our reconstructed area/volume sometimes is partial or not cylinder-like), therefore the observed distortion is larger since the model in [10] assumes that the 3D fingerprints can be segmented into slices like from the cylindrical portions. The difference in the heights of the ridge and valley is also observed to be smaller on the edges of the reconstructed 3D fingerprints since our imaging setup uses the camera at the top/vertex (also such part of the valley is often occluded by ridges on the edges of 3D fingerprints).

We also employed the 2D minutiae quality [6], corresponding to the matched 3D minutiae during score generation in (15) and attempted to achieve performance improvement. However, as can be seen from the results in figure 5, such an approach was not successful. This can be possibly attributed to the fact that 2D minutiae quality may be not be a reliable indicator for 3D minutiae quality and an independent indicator needs [4] to be developed for 3D minutiae quality in the further work.

The matching scores generated from 2D fingerprint images, acquired for the 3D fingerprint reconstruction, can be combined with the 3D fingerprint matching scores to

achieve performance improvement. As detailed in section 3.1 and 3.2, we explored 3D fingerprint matching using the 3D surface curvature information and the 3D minutiae (figure 5). We comparatively explored the score level combination of 3D surface curvature scores and 3D minutiae matching scores with those from simultaneously generated 2D fingerprint matching scores (section 3.3).

The experimental results from 240 client's fingerprints using 3600 genuine and 2064960 impostor scores are shown in figure 7. The EER using 2D minutiae matching was 2.12%, which reduced to 1.73% when combined with 3D curvature match scores and to 1.17% when combined with 3D minutiae match scores (nonlinear fusion [23]). It can be observed that the combination of 3D minutiae and 2D minutiae matching scores can significantly improve the performance, as compared to those for the combination with 3D curvature matching scores. The experimental results thus illustrate merit in utilizing *shape from shading* images (2D minutiae) along with the recovered 3D minutiae, for improving the matching accuracy.

5. Conclusions and Further Work

This paper has developed a low-cost 3D fingerprint identification system using a single camera and presented promising results on the database of 1440 3D fingerprints acquired from 240 clients in this study. Comparative experimental results presented in this paper (figure 2, 5) illustrate their superiority over matching approaches presented in [10], [16].

Fingerprint minutiae features are widely considered to be most reliable and employed in most of the commercial and forensic fingerprint systems available today. Our efforts to further ascertain their distinctiveness by incorporating minutiae height z and their 3D orientation ϕ have shown most promising results while matching 3D fingerprints. Intra-class variations in 3D fingerprints are accounted by *aligning* every recovered 3D minutiae with respect to a reference (origin, figure 3-4), using a tolerance band and then using the best matching scores from (15).

Despite promising results and success in developing a low-cost 3D fingerprint solution, one paper cannot address several open issues in this area which require further research efforts. The performance from 3D fingerprint minutiae matching is lower than those achieved from the 2D minutiae in our experiments. There can be two plausible explanations for such discrepancy. Firstly, all the seven 2D fingerprint images are employed to generate 2D minutiae matching scores while only one reconstructed 3D fingerprint is used for generating 3D minutiae matching performance. Secondly, the reconstruction error in the 3D fingerprint surface reconstruction can degrade 3D minutiae matching performance. Further improvement in the reconstruction accuracy is expected to further improve the performance from the 3D minutiae matching and should be explored in the further extension of this work.

References

[1] D. Maltoni, D. Maio, A. K. Jain, S. Prabhakar, *Handbook of Fingerprint Recognition*, Springer, Jun. 2009.

[2] G. Parziale and Y. Chen, "Advanced technologies for touchless fingerprint recognition," *Handbook of Remote Biometrics*, M. Tistarelli, Stan. Z. Li, R. Challeppa, (*Eds.*), pp. 83-109, Springer-Verlag London, 2009.

[3] P. Krishnasmy, S. Belongie, D. Kriegman, "Wet Fingerprint Recognition: Challenges and Opportunities," *Proc. IJCB 2011*, Washington, DC, October, 2011.

[4] P. Grother and E. Tabassi, "Performance of biometric quality evaluations," *IEEE Trans. PAMI*, vol. 29, pp. 531–543, 2007.

[5] The Hong Kong Polytechnic University 3D Fingerprint Images Database,2013
http://www.comp.polyu.edu.hk/~csajaykr/3Dfingerprint.htm

[6] NIST Biometric Image Software, NBIS Release 4.1.0, http://www.nist.gov/itl/iad/ig/nbis.cfm, 2011.

[7] R. T. Frankot and R. Chellappa, "A method for enforcing integrability in shape from," *Proc. ICCV*, 1987.

[8] A. Kumar and Y. Zhou, "Contactless fingerprint identification using level zero features," *Proc. CVPR 2011*, Colorado Springs, CVPR'W 2011, pp. 121-126, Jun. 2011.

[9] W. J. Scheirer, A. Rocha, R. Micheals, T. E. Boult, "Meta-Recognition: The theory and practice of recognition score analysis," *T- PAMI*, vol. 33, pp. 1689-1695, Aug. 2011.

[10] Y. Wang, L. G. Hassebrook, D. L. Lau, "Data acquisition and processing of 3-D fingerprints," *T-IFS*, pp, 750-760, Dec. 2010.

[11] A. K. Jain, S. Prabhakar, L. Hong, S. Pankanti, "Filterbank-based fingerprint matching," *T- IP*, pp. 846-859, 2000.

[12] C. Dorai and A. K. Jain, "COSMOS—A representation scheme for 3D free-form objects," *T-PAMI*, pp. 1115-1130, 1997.

[13] Y. Chen, G. Parziale, E. Diaz-Santana, and A. K. Jain, "3D Touchless fingerprints: Compatibility with legacy rolled images," *Proc. BCC 2006*, Tampa, 2006.

[14] J. Goldfeather and V. Interrante, "A novel cubic-order algorithm for approximating principal direction vectors," *ACM Trans. Graphics*, vol. 23, no. 1, pp. 45-63, 2004.

[15] *Shape from Shading*, B. K. P. Horn and M. J. Brooks (*Eds.*), MIT Press, Cambridge, MA, 1989.

[16] V. Kanhangad, A. Kumar, D. Zhang, "A unified framework for contactless hand identification," *T- IFS*, pp. 1414-25, May 2011.

[17] A. Belyaev, "Mesh Smoothing and Enhancing. Curvature Estimation," Saarbrucken, 2006.
www.mpi-inf.mpg.de/~ag4-gm/handouts/06gm_surf3.pdf

[18] G. Parziale, E. Diaz-Santana and R. Hauke, "The surround imager: A multi-camera touchless device to acquire 3d rolled-equivalent fingerprints," *Proc. ICB 2006*, vol. 3832, Jan 2006.

[19] A. Agrawal, R. Raskar and R. Chellappa, "What is the range of surface reconstructions from a gradient field?," *Proc. 9th ECCV*, Graz, Austria, May 2006.

[20] TBS, http://www.tbs-biometrics.com, Accessed Oct 2012

[21] FlashScan, http://www.FlashScan3D.com, Accessed Oct 2012

[22] Y. Wang, D. L. Lau and L. G. Hassebrook, "Fit-sphere unwrapping and performance analysis of 3D fingerprints," Applied Optics, vol. 49, no. 4, pp. 592-600, 2010.

[23] A. Kumar and Y. Zhou, "Human identification using finger images," *T- IP*, vol. 21, pp. 2228-2244, Apr. 2012.

[24] Y. Wang, Q. Hao, A. Fatehpuria, D. L. Lau, L. G. Hassebrook, "Data acquisition and quality analysis of 3-Dimensional fingerprints*," Proc. IEEE conference on Biometrics, Identity and Security*, Tampa, Florida, Sep. 22-24, 2009

[25] J. Daugman, "High confidence visual recognition of persons by a test of statistical independence," *T-PAMI*, vol. 15, pp. 1148-1161, 1993.